# Probing the effect of magnetic field on charge order in the quasi-two-dimensional Mott insulator $\kappa$-$(ET)_2Hg(SCN)_2Cl$

Nora M. Hassan,[1,2] Komalavalli Thirunavukkuarasu,[3] Zhengguang Lu,[4,5] Dmitry Smirnov,[4] Elena I. Zhilyaeva,[6] Svetlana Torunova,[6] Rimma N. Lyubovskaya,[6] and Natalia Drichko[1,*]

[1]*Institute for Quantum Matter and Department of Physics and Astronomy, Johns Hopkins University, Baltimore, Maryland 21218, USA*
[2]*Department of Chemical & Biological Engineering, Iowa State University, Ames, Iowa 50011, USA*
[3]*Department of Physics, Florida AM University, Tallahassee, Florida 32307, USA*
[4]*National High Magnetic Field Laboratory, Tallahassee, Florida 32310, USA*
[5]*Department of Physics, Florida State University, Tallahassee, Florida 32306, USA*
[6]*Institute of Problems of Chemical Physics, Chernogolovka 142432, Russia*

(Received 4 March 2021; revised 22 October 2021; accepted 30 November 2021; published 13 December 2021)

Molecular-based quasi-two-dimensional charge-ordered Mott insulators can possess both spin $S = 1/2$ and an electric dipole degree of freedom residing on each $(BEDT\text{-}TTF)_2$ lattice site. There exists a theoretical proposal for a magnetoelectric effect in such a material, which can manifest itself as a sensitivity of charge distribution on $(BEDT\text{-}TTF)_2$ dimers to the magnetic field. In this work, we used Raman scattering spectroscopy in the magnetic field up to 31 T applied perpendicular to the two-dimensional triangular lattice planes to probe a magnetoelectric effect in $\kappa$-$(ET)_2Hg(SCN)_2Cl$. This is a model compound, which shows charge order and antiferromagnetic correlations at temperatures below 30 K. We discuss possible reasons for the absence of an observable magnetoelectric effect in the probed temperature and magnetic field ranges.

DOI: 10.1103/PhysRevB.104.245120

## I. INTRODUCTION

Much of the current research in condensed matter physics is focused on the emergent states of matter resulting from electronic correlations and magnetic interactions. In Mott insulators with commensurate band fillings away from 1/2, such as 1/4 or 1/3, strong electronic correlations can result in a charge-order state [1–3]. In molecular-based Mott insulators where the lattice has a suitable commensurate periodicity, such as dimerization, charge order can lead to the formation of electric dipoles without a need to additionally break the lattice symmetry, resulting in electronic ferroelectricity [4]. Such a condition can be realized in ET-based [ET is the bis(ethylenedithio)tetrathiafulvalene molecule] Mott insulators. Indeed, electronic ferroelectricity due to charge order has been observed in $\kappa$-$(ET)_2Hg(SCN)_2Cl$ [5,6].

Unpaired electrons forming the charge-order pattern carry spin $S = 1/2$; therefore, a coupling of charge and magnetic degrees of freedom is expected for these materials. Multiferroic behavior of dimerized organic Mott insulators without well-pronounced charge order was detected by following the correlation of dielectric and magnetic responses [7–9]. This coupling was also suggested as a way to obtain a quantum spin liquid state out of fluctuating electric dipoles [10]. Fluctuating electric dipoles were suggested experimentally in systems that also do not order magnetically [11–14], despite antiferromagnetic interactions of the order of at least 100 K [15].

Coupling of the charge and spin degrees of freedom can manifest in two ways. First, a ground state of the charge degree of freedom will define a magnetic ground state. For example, a charge-ordered ferroelectric state in a quasi-two-dimensional molecular material can result in a spin singlet in the case of an additional lattice distortion [16] or antiferromagnetic $S = 1/2$ chains in the absence of coupling to the lattice [4]. Second, a coupling between charge and spin can manifest itself in a magnetoelectric effect, where an application of the electric field would change the magnetization of an ordered system [17] or an application of the magnetic field would affect the charge degree of freedom.

$\kappa$-$(ET)_2Hg(SCN)_2Cl$ is a realistic candidate for a magnetoelectric effect in molecular Mott insulators theoretically suggested in Ref. [17]. In this layered crystal, the cation layers are formed by the $(ET)_2^{1+}$ dimers arranged into an anisotropic triangular lattice. This material demonstrates a charge-ordered insulating state below 30 K [5,6,12], which shows signatures of electronic ferroelectricity [6] without a formation of a nonmagnetic spin singlet state [14] as was observed in materials with larger charge disproportionation, for example, $\theta$-$(ET)_2RbZn(SCN)_2$ [18]. Electric dipole moments are formed on $(ET)_2^{1+}$ dimer lattice sites due to charge disproportionation within the dimers. This charge order melts below 15 K, where an inhomogeneous charge state is observed, driven presumably by the vicinity to the charge-order phase transition [12,13]. $\kappa$-$(ET)_2Hg(SCN)_2Cl$ shows an absence of magnetic order down to at least 70 mK [14,19] despite antiferromagnetic interactions on the order of 100 K [15]. While no long-range magnetic order has been detected, a decrease of magnetic susceptibility below 24 K and an agreement in temperature dependence of charge and magnetic properties [14] suggest short-range magnetic correlations and coupling between the magnetic and charge degrees of freedom.

*drichko@jhu.edu

 

We used Raman scattering spectroscopy and heat capacity in the applied magnetic field to search for a possible effect of the magnetic field on charge order in $\kappa$-$(ET)_2Hg(SCN)_2Cl$. Vibrational Raman spectroscopy is the technique of choice to search for a change in charge distribution on the lattice upon the application of the magnetic field for the following reason. In an ET-molecule-based system it is possible to follow the charge degree of freedom and the charge distribution on the lattice by the measurements of the charge-sensitive Raman-active vibration $\nu_2(A_g)$ (vibration of the central C = C bond of ET molecules). The sensitivity of this method has been proven in many cases [20,21] including the detection of the charge-ordered state and low-temperature melting of the charge order in $\kappa$-$(ET)_2Hg(SCN)_2Cl$ [12]. We followed the charge-sensitive vibrations of ET on the application of the magnetic field up to 31 T, directed perpendicular to the planes formed by $(ET)_2^{1+}$ dimers [see Fig. 1(a)]. Even at the highest reached field, we have not detected any changes of the spectra that can be clearly interpreted as changes of the charge state, neither in the charge-ordered state nor in the melted low-temperature state. We do not observe any change of the low-temperature heat capacity on the application of the magnetic field up to 14 T within the precision of our measurements. This result can lead to further understanding of the coupling between charge and spin degrees of freedom in these molecular Mott insulators.

## II. EXPERIMENT

Single crystals of $\kappa$-$(ET)_2Hg(SCN)_2Cl$ were prepared by electrochemical oxidation of the ET solution in 1,1,2-trichloroethane at a temperature of 40 °C and a constant current of 0.5 $\mu A$. The composition of the crystal was verified by electron probe microanalysis and x-ray diffraction. The crystal structure [5] of $\kappa$-$(ET)_2Hg(SCN)_2Cl$ consists of $(ET)_2^{1+}$-based cation layers and anion layers parallel to the *bc* crystallographic plane, with the *a* axis perpendicular to the layers. In the *bc* planes, $(ET)_2^{1+}$ dimers form anisotropic triangular lattice, which is schematically shown in the right-hand panels of Fig. 1.

Magneto-Raman measurements of $\kappa$-$(ET)_2Hg(SCN)_2Cl$ were performed at National High Magnetic Field Lab using a fiber-based probe and a $^4$He exchange gas cryostat and two different magnets. A superconducting magnet was used to reach magnetic fields up to 18 T, with a minimum temperature on the sample of 2 K and a cooling rate between 1 and 8 K/min. A resistive magnet was used to reach magnetic fields up to 31 T, with a minimum temperature on the sample of 3.5 K and a cooling rate about 1 K/min. The Raman spectra were measured in a backscattering geometry using a 532-nm laser excitation. The laser light was injected into an single-mode optical fiber, guiding the excitation to the sample stage inserted into a helium-flow variable temperature cryostat. The excitation light was focused by an aspheric objective lens (NA = 0.67) to a spot size of about 3.5 $\mu$m in diameter. The excitation power delivered to the sample was about 100 $\mu$W or less to minimize the sample heating. The scattered light collected by the same lens was directed into a 100-$\mu$m multimode collection fiber and then guided to a spectrometer equipped with a liquid-nitrogen-cooled CCD camera. The spectra were acquired in the spectral region from 1200 to 1700 $cm^{-1}$ with a spectral resolution of 1.74 $cm^{-1}$. Nonpolarized Raman scattering spectra were measured from the *bc* plane of the crystals with the wave vector of the excitation and scattered light oriented perpendicular to the layers. The magnetic field was oriented perpendicular to the *bc* plane.

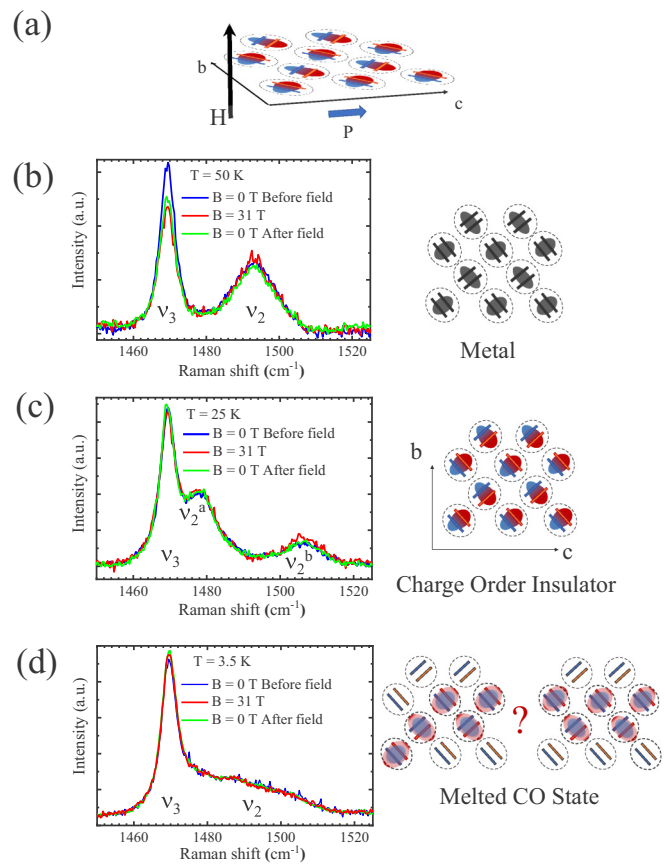


FIG. 1. (a) A scheme of the $(ET)_2^{1+}$ layer parallel to the *bc* plane in the charge-ordered state. $(ET)_2^{1+}$ dimers are shown schematically by dashed circles, with a charge-rich (red) and a charge-poor (blue) molecule in a dimer in a charge-ordered state. *P* is the vector of electric polarization as deducted from the evidence of charge-order stripes parallel to the *c* axis observed in Refs. [5,6]. *H* is the direction of the applied magnetic field. (b)–(d) Raman spectra of $\kappa$-$(ET)_2Hg(SCN)_2Cl$ in the region of charge-sensitive molecular vibration $\nu_2(A_g)$ at 0 and 31 T. For all temperatures, measurements taken at 0 T are plotted by a blue curve ("Before field"), at 31 T field by a red curve, and at 0 T after application of high field by a green curve ("After field"). Right-hand panels show schematically the charge distribution in the $(ET)_2^{1+}$ layer. (b) Spectra in the metallic state at 50 K. No effect of the magnetic field on the shape of the charge sensitive $\nu_2(A_g)$ vibration is observed. In the metallic state, charge is distributed homogeneously between molecules in the dimers (depicted by black color). (c) Spectra in the charge-ordered state at 25 K. $\nu_2^a(A_g)$ and $\nu_2^b(A_g)$ lines correspond to charge-rich and charge-poor molecular sites. Upon the application of 31 T, no change is observed. (d) Spectra in the charge melting state at 3.5 K. There is no appreciable difference between spectra taken at zero field and spectra at 31 T. The right panel shows the inhomogeneous $(ET)_2^{1+}$ layer, where part of the system recovered homogeneous charge distribution. The domains of both phases can have random shapes or be oriented parallel to the charge-ordered stripes.

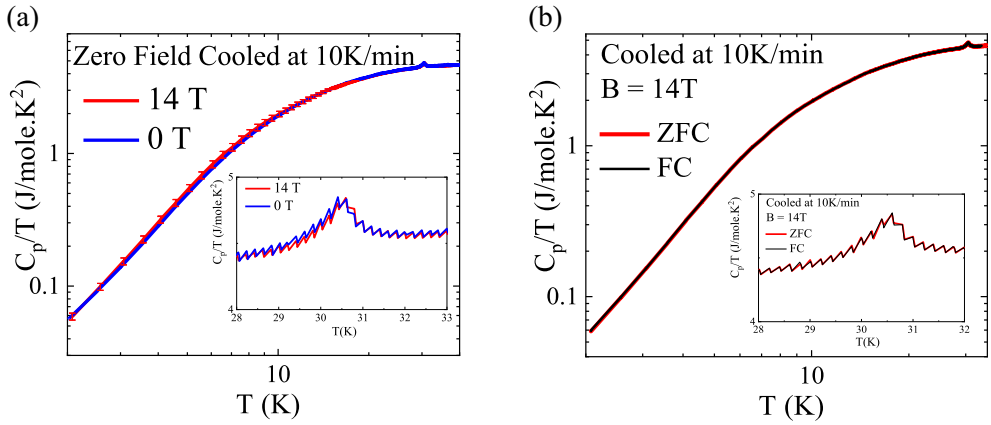


FIG. 2. Temperature dependence of heat capacity of $\kappa$-$(ET)_2Hg(SCN)_2Cl$ plotted as $C_p/T$ vs $T$. (a) The blue curve is the heat capacity at zero magnetic field and the red curve is heat capacity measurements taken at 14 T. No detectable difference was noticed either at low temperature or at the transition temperature. (b) Plot of $C_p/T$ vs $T$ at 14 T. The red curve is the heat capacity of the sample that was cooled down in zero field. The black curve is the heat capacity of sample that was cooled down in a field of 14 T.

The heat capacity of three different crystals of $\kappa$-$(ET)_2Hg(SCN)_2Cl$ with masses of 0.56, 1.11, and 0.93 mg were measured using Quantum Design PPMS (relaxation method). Samples have shapes of thin plates with the most developed *bc* plane. The samples were fixed on the measurement platform using Apiezone N grease. Measurements were performed with a few different cooling rates between 0.1 and 10 K/min. No difference in heat capacity measured with these cooling rates was observed within the precision of our measurements. In Fig. 2 we present the data obtained using a cooling rate of 10 K/min.

In the heat capacity measurements, a magnetic field up to 14 T was applied in the direction perpendicular to the *bc* plane of the crystals. The heat capacities of the sample in the field of 14 T and in 0 T show some difference of a few percent below about 15 K. This difference follows the difference observed in the addenda measurements in this temperature range and therefore is considered a systematic error, which gives rise to the increased error bars defined as $C_p(\text{sample at } 14\,\text{T}) = C_p(\text{sample at } 14\,\text{T}) * \frac{C_p(\text{addenda at } 14\,\text{T})}{C_p(\text{addenda at } 0\,\text{T})}$ and plotted in Fig. 2.

The zero-field-cooled (ZFC) heat capacity was measured in the magnetic field upon warming. Field-cooled measurements at 14 T were done upon cooling.

## III. RESULTS

In our Raman scattering experiments, we were following the charge distribution on $(ET)_2^{1+}$ dimers of $\kappa$-$(ET)_2Hg(SCN)_2Cl$ by probing the $\nu_2(A_g)$ vibration of the central C = C bond of ET molecules. The dependence of the frequency of this vibration on the charge on the ET molecules is well known [12,22]. Another vibration detected in the measured range is $\nu_3(A_g)$, which is not sensitive to changes of the charge on a ET molecule and is used for calibration. Raman spectra were measured at a few different temperatures which correspond to different charge states observed in $\kappa$-$(ET)_2Hg(SCN)_2Cl$. All zero-field data are in agreement with the previous Raman scattering studies of this material [12]. In Fig. 1 we show the results obtained in the measurements using a resistive magnet and a maximum applied field of 31 T. The data obtained in the measurements using a superconducting magnet and magnetic fields up to 18 T are in agreement with these data and are presented in the Appendix Fig. 3. At each measured temperature, Raman scattering spectra were taken in the magnetic field $H = 0$ T (marked as "Before field" in Fig. 1) and then at the maximum value of 31 T in order to detect a possible influence of the magnetic field on the charge state. Then the magnetic field was decreased down to 0 T, and another Raman spectrum was taken (marked as "After field" in Fig. 1). Differential spectra are also presented in Fig. 4 in the Appendix.

Above 30 K, $\kappa$-$(ET)_2Hg(SCN)_2Cl$ is known to be a metal with a homogeneous distribution of charge on the lattice [5]. Figure 1(b) shows Raman spectra of the metallic state at $T = 50$ K, where a single band of the $\nu_2(A_g)$ vibration is detected at a frequency of 1490 $cm^{-1}$. At the maximum magnetic field of 31 T we observe no changes of the $\nu_2(A_g)$ mode; however, the intensity of the $\nu_3(A_g)$ mode at 1470 $cm^{-1}$ decreased. Raman spectra measured after removing the field and repeating the measurements in $H = 0$ T are almost identical to that measured under the magnetic field of 31 T. This suggests that the observed decrease of intensity could be attributed to the movement of the piezo stage of the sample holder or parts of the optics that affected positioning of the sample or the focus (see the Appendix Fig. 4 for more details), with $\nu_3$ being more sensitive to the exact positioning due to resonance effects [23].

In the charge-ordered state, represented by the spectra at $T = 25$ K [see Fig. 1(c)], the line of the charge-sensitive $\nu_2$ vibration splits into two modes, $\nu_2^a(A_g)$ at 1475 $cm^{-1}$ and $\nu_2^b(A_g)$ at 1507 $cm^{-1}$, corresponding to charge-rich (carrying $+0.6e$) and charge-poor (carrying $+0.4e$) molecules within a dimer. Charge-rich and charge-poor molecules of a dimer are depicted schematically by red and blue colors in the right panel of Fig. 1(c). While the maximum magnetic field of 31 T is comparable to the temperature of the charge-order transition $T_{MI} = 30$ K, we observed no apparent changes of the charge-sensitive vibrations in the magnetic field up to 31 T. A small change of the intensity of $\nu_2^b(A_g)$ is within the error of the measurements. This suggests an absence of a detectable influence of the magnetic field on

the charge state of $\kappa$-$(ET)_2Hg(SCN)_2Cl$ in this geometry at least.

As was demonstrated in Ref. [12], below 15 K, $\kappa$-$(ET)_2Hg(SCN)_2Cl$ enters the charge melted regime where the intensity of the vibrational bands related to the charge order start to gradually decrease upon cooling, while that of the mode $\nu_2(A_g)$ of $(ET)^{0.5+}$ increases. We probed this state at $T = 3.5$ K, where the $\nu_2(A_g)$ mode is very broad [see Fig. 1(d)]. An application of the magnetic field up to 31 T does not affect the spectra.

In addition to the Raman scattering experiments, we performed heat capacity measurements of $\kappa$-$(ET)_2Hg(SCN)_2Cl$ in the magnetic field up to 14 T applied in the same geometry, perpendicular to the *bc* crystallographic plane. The temperature dependence of $C_p/T$ vs $T$ is shown in Fig. 2. The feature at 30 K is associated with the charge-order metal-insulator transition and is in agreement with previous results [6,11].

Figure 2(a) shows a comparison between the heat capacity at zero field and the heat capacity at 14 T. The heat capacities of the sample in the field at 14 T and at 0 T show some difference of a few percent below about 15 K. This difference follows the difference observed in the addenda measurements in this temperature range and therefore is considered a systematic error, which gives rise to increased error bars defined as $C_p(\text{sample at } 14\,\text{T}) = C_p(\text{sample at } 14\,\text{T})\frac{C_p(\text{addenda at } 14\,\text{T})}{C_p(\text{addenda at } 0\,\text{T})}$ and plotted in Fig. 2.

Figure 2(b) is a comparison between heat capacity measurements taken at 14 T for a zero field cooling and field cooling, again showing no difference between the heat capacity measured in these two regimes.

## IV. DISCUSSION

The main result of our measurements of Raman scattering spectra in the magnetic field up to 31 T applied perpendicular to the *bc* crystallographic plane is the absence of any changes of the spectra which we can reliably interpret as a change of the charge distribution on $(ET)_2^{1+}$ dimers in $\kappa$-$(ET)_2Hg(SCN)_2Cl$ induced by the application of the magnetic field. An absence of a change in heat capacity in the magnetic field up to 14 T applied in the same geometry confirms this result.

There could be a number of reasons why the observation of a magnetoelectric effect is absent. The suggestion of the magnetoelectric effect in a charge-ordered organic Mott insulator in Ref. [17] is based on the assumption of a non-negligible spin-charge coupling, which would also lead to magnetic ordering, that can appear at temperatures lower than charge order. Reference [14] suggests that spin-charge separation due to the one-dimensional character of the charge stripes can be a reason for the absence of magnetic order accompanying the charge-order phase transition. In fact, the one-dimensionality of the system in the charge-ordered state was suggested by experimental results in Ref. [6] and theoretical calculations in Ref. [15]. This could explain the absence of the magnetoelectric effect at $T = 25$ K.

At $T = 23$ K, magnetic susceptibility shows a decrease presumably due to short-range magnetic correlations [14]. Below this temperature, magnetic susceptibility follows the temperature behavior of the charge degree of freedom. Melted charge order and an absence of magnetic order are observed at low temperatures [14,19]. This temperature regime seems to be a better candidate for the magnetoelectric effect. However, at $T = 3.5$ K no effect was observed. It is possible that spin-charge coupling in this regime is still not strong enough to produce an observable magnetoelectric effect, or that a stable magnetic order, and not a fluctuating regime, is necessary.

Another possibility is that the magnetic field of 31 T is still too weak to produce any detectable effect on the charge order. While this energy of the magnetic field is comparable to the temperature of the charge-order transition, it is smaller than the estimations of $J$ in such a system, the lowest of which is 80 K [11,24]. Theoretical calculations are necessary to estimate how parameters related to the charge and magnetic degrees of freedom compare to the magnetic field that can produce a detectable magnetoelectric effect.

In contrast, the magnetic field produces a strong effect in the NMR response of $\kappa$-$(ET)_2Hg(SCN)_2Cl$, suppressing a maximum in $T_1^{-1}$ in the temperature range below approximately 10 K [19]. Our data on the absence of the effect of the magnetic field on the charge order reinforce the conclusion of Ref. [19] that it is the impurity spins that show a strong magnetic field dependence. The melting of charge order observed below 15 K undoubtedly creates inhomogeneities and domain walls, which can produce the strong field dependence observed in NMR experiments.

Temperature dependence of the heat capacity of $\kappa$-$(ET)_2Hg(SCN)_2Cl$ (see Fig. 2) is not affected by the application of a magnetic field up to 14 T. This confirms the Raman scattering-based conclusion that $\kappa$-$(ET)_2Hg(SCN)_2Cl$ is not affected by these values of magnetic fields. A comparison to the NMR results also suggests that domain walls and the related orphan spins do not have a measurable input into the heat capacity of $\kappa$-$(ET)_2Hg(SCN)_2Cl$.

## V. CONCLUSIONS

In this work we have tested a possible effect of the magnetic field on charge distribution on $(ET)_2^{1+}$ dimers in $\kappa$-$(ET)_2Hg(SCN)_2Cl$, which was predicted as a realization of the magnetoelectric effect. This was done by application of a magnetic field perpendicular to the $(ET)_2^{1+}$ layers and following the response of the charge distribution on $(ET)_2^{1+}$ dimers through Raman vibrational spectra. We have not observed any evidence of a magnetoelectric effect that would affect charge distribution in the insulating charge-order state in a magnetic field up to 31 T. We suggest possible reasons for the absence of a magnetoelectric effect. Those include a possibility that the energy of the magnetic field should be much higher and comparable to the magnetic exchange to produce an effect. Also, a magnetoelectric effect might require a stronger coupling between charge and spin degrees of freedom, which would also manifest itself in a spin order accompanying the charge-order state.

## ACKNOWLEDGMENTS

Work in JHU was supported as part of the Institute for Quantum Matter, an Energy Frontier Research Center funded

by the U.S. Department of Energy, Office of Science, Office of Basic Energy Sciences under Grant No. DE-SC0019331. The work in Chernogolovka was performed in accordance with the state task, State Registration No. AAAA-A19-119092390079-8. K.T. acknowledges funding from the DoN HBCU/MI program, Grant No. N00014-17-1-3061. A portion of this work was performed at the National High Magnetic Field Laboratory, which is supported by the National Science Foundation under Cooperative Agreement No. DMR-1644779 and by the State of Florida. N.D. and N.H. acknowledge the support of the Institute for Complex Adaptive Matter (ICAM) and The Gordon and Betty Moore Foundation.

## APPENDIX

As mentioned in the main text of the paper, the measurements of Raman scattering spectra in the magnetic field were performed at two setups, one was equipped with an 18 T superconducting magnet, and another was equipped with a 31 T resistive magnet. In Figs. 3 and 4 we demonstrate a

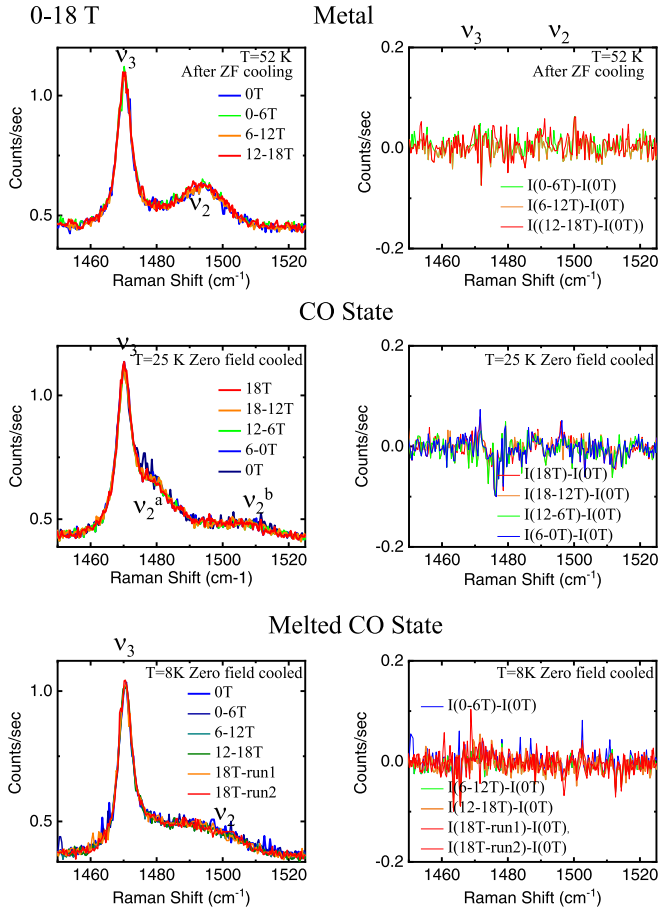


FIG. 3. $H = 18$ T setup: Raman spectra of $\kappa$-$(ET)_2Hg(SCN)_2Cl$ in the region of charge-sensitive molecular vibration $\nu_2(A_g)$ at three different temperatures which correspond to three different charge states: $T = 52$ K is a metallic state, $T = 25$ K is a charge-ordered state, and $T = 8$ K is a state where charge order is melted. Each temperature shows spectra in the magnetic field, some are measured on sweeps between two fields. The right panels show a difference of intensity between the spectra in field and at zero field for a given temperature.

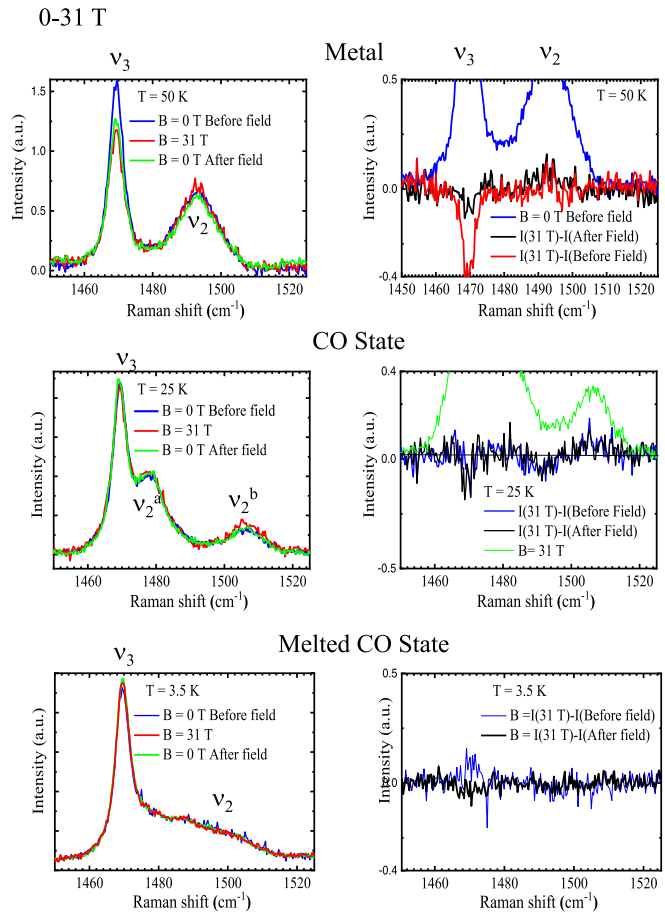


FIG. 4. $H = 31$ T setup: Raman spectra of $\kappa$-$(ET)_2Hg(SCN)_2Cl$ in the region of charge-sensitive molecular vibration $\nu_2(A_g)$ at three different temperatures which correspond to three different charge states: $T = 50$ K is a metallic state, $T = 25$ K is a charge-ordered state, and $T = 3.5$ K is a state where charge order is melted. Each temperature shows spectra in the magnetic field, some are measured on sweeps between two fields. The right panels show a difference of intensity between the spectra in field and at zero field for a given temperature.

set of original data for both measurements taken at temperatures which correspond to the three states observed in the $\kappa$-$(ET)_2Hg(SCN)_2Cl$ metal (50 K), the charge-ordered state (25 K), and the melted charge order (8 K for the 18 T setup and 3.5 K for the 31-T setup). Fig. 5 summarizes the differential spectra for the three studied temperature regimes.

The small changes in the spectra observed in field are identified the best in the plots of $I(H) - I(0\,\mathrm{T})$ presented in the right panels of the figures for each temperature. For both systems and all temperatures we observe the changes in the intensity of the $\nu_3$ mode. While changes at higher field are larger, the sign and size of the changes are not systematic. For the measurements at 18 T and below, the changes are below the noise observed in the spectra (see the right-hand panels of Fig. 3).

In the case of measurements at the 31 T setup at 50 and 3.5 K, 0 T intensities of the $\nu_3$ mode before and after the field sweep are not reproduced. This suggest that the changes of the intensities are due to small shifts of the sample or

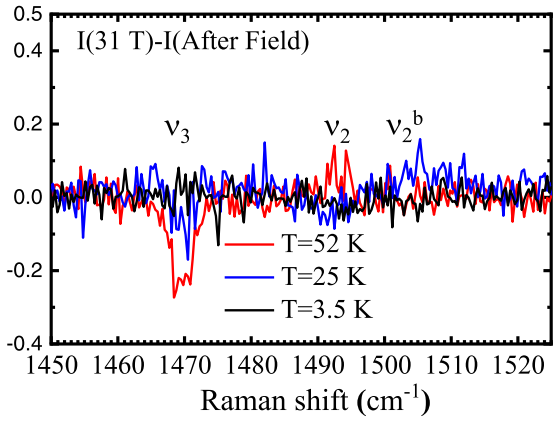


FIG. 5. Averaged values of spectral changes in field $\frac{[I(31\,\mathrm{T})-I(0\,\mathrm{T}\ \text{“before field”})]+[I(31\,\mathrm{T})-I(0\,\mathrm{T}\ \text{“after field”})]}{2}$ for three different temperatures: $T = 50$ K (metallic state), $T = 25$ K (charge-ordered state), and $T = 3.5$ K (melted charge-order state).

sample holder in high field, as well as polarization rotation, and cannot be assigned to the intrinsic behavior of the sample.

Changes of the intensity of the $\nu_2$ mode are observed in the spectra at 31 T for $T = 50$ and 25 K. The changes at 50 K show an increase of the intensity of the $\nu_2$ mode. A decrease of $I(\nu_3)$ together with an increase of $I(\nu_2)$ is in agreement with a polarization rotation, since these $A_g$ vibrations are observed in the two perpendicular polarizations $(c, c)$ and $(b, b)$ in the $bc$ plane of the $\kappa$-$(ET)_2Hg(SCN)_2Cl$ structure [23]. This suggests that changes at 52 K are a combination of a sample shift in high magnetic fields and polarization rotation.

In the spectra at $T = 25$ K, $I(\nu_3)$ decreases, while $I(\nu_2)$ decreases as well, with an increase of $I(\nu_3^b)$. To appreciate this change we plot together $I(31\,\mathrm{T}) - I(0\,\mathrm{T})$ for each temperature, averaged over $I(31\,\mathrm{T}) - I(0\,\mathrm{T}$ “before field”) and $I(31\,\mathrm{T}) - I(0\,\mathrm{T}$ “after field”). Such a change can point to a decrease of charge from BEDT-TTF$^{+0.5}$ to BEDT-TTF$^{+0.4}$ on the application of $H = 31$ T in a small part of the system. This interpretation would mean that there are some non-charge-ordered molecules with BEDT-TTF$^{+0.5}$ left in the charge-ordered state at $T = 25$ K. Another concern is that we do not observe a corresponding change in $I(\nu_3^a)$ of BEDT-TTF$^{+0.6}$ necessary to keep the charge equilibrium. As a whole, taking into account the size of the noise and the possible artifacts discussed above, we cannot interpret this effect as a significant change.

Interestingly, no changes are observed in the magnetic field at $T = 3.5$ K. This can be interpreted as a result of higher mechanical stability of the system at low temperatures, or an absence of polarization dependence in the melted charge-order state. It can also signify the changes observed in the system at higher temperatures.


[1] T. Takahashi, Y. Nogami, and K. Yakushi, J. Phys. Soc. Jpn. **75**, 051008 (2006).
[2] C. N. R. Rao, A. Arulraj, P. N. Santosh, and A. K. Cheetham, Chem. Mater. **10**, 2714 (1998).
[3] M. Dressel and S. Tomić, Adv. Phys. **69**, 1 (2020).
[4] M. Naka and S. Ishihara, J. Phys. Soc. Jpn. **79**, 063707 (2010).
[5] N. Drichko, R. Beyer, E. Rose, M. Dressel, J. A. Schlueter, S. A. Turunova, E. I. Zhilyaeva, and R. N. Lyubovskaya, Phys. Rev. B **89**, 075133 (2014).
[6] E. Gati, J. K. H. Fischer, P. Lunkenheimer, D. Zielke, S. Kohler, F. Kolb, H. A. K. von Nidda, S. M. Winter, H. Schubert, J. A. Schlueter, H. O. Jeschke, R. Valenti, and M. Lang, Phys. Rev. Lett. **120**, 247601 (2018).
[7] M. Abdel-Jawad, I. Terasaki, T. Sasaki, N. Yoneyama, N. Kobayashi, Y. Uesu, and C. Hotta, Phys. Rev. B **82**, 125119 (2010).
[8] P. Lunkenheimer, J. Müller, S. Krohns, F. Schrettle, A. Loidl, B. Hartmann, R. Rommel, M. De Souza, C. Hotta, J. A. Schlueter *et al.*, Nat. Mater. **11**, 755 (2012).
[9] M. Poirier, S. Parent, A. Côté, K. Miyagawa, K. Kanoda, and Y. Shimizu, Phys. Rev. B **85**, 134444 (2012).
[10] C. Hotta, Phys. Rev. B **82**, 241104(R) (2010).
[11] N. Hassan, S. Cunningham, M. Mourigal, E. I. Zhilyaeva, S. A. Torunova, R. N. Lyubovskaya, J. A. Schlueter, and N. Drichko, Science **360**, 1101 (2018).
[12] N. M. Hassan, K. Thirunavukkuarasu, Z. Lu, D. Smirnov, E. I. Zhilyaeva, S. Torunova, R. N. Lyubovskaya, and N. Drichko, npj Quantum Mater. **5**, 15 (2020).
[13] M. Yamashita, S. Sugiura, A. Ueda, S. Dekura, T. Terashima, S. Uji, Y. Sunairi, H. Mori, E. I. Zhilyaeva, S. A. Torunova *et al.*, npj Quantum Mater. **6**, 87 (2021).
[14] N. Drichko, S. Sugiura, M. Yamashita, A. Ueda, S. Uji, N. Hassan, Y. Sunairi, H. Mori, E. I. Zhilyaeva, S. Torunova *et al.*, arXiv:2102.11342.
[15] A. C. Jacko, E. P. Kenny, and B. J. Powell, Phys. Rev. B **101**, 125110 (2020).
[16] S. Dayal, R. T. Clay, H. Li, and S. Mazumdar, Phys. Rev. B **83**, 245106 (2011).
[17] M. Naka and S. Ishihara, Sci. Rep. **6**, 20781 (2016).
[18] H. Mori, S. Tanaka, T. Mori, and A. Fuse, Synth. Met. **86**, 1789 (1997).
[19] A. Pustogow, T. Le, H.-H. Wang, Y. Luo, E. Gati, H. Schubert, M. Lang, and S. E. Brown, Phys. Rev. B **101**, 140401(R) (2020).
[20] K. Yakushi, Crystals **2**, 1291 (2012).
[21] K. Yakushi, K. Yamamoto, T. Yamamoto, Y. Saito, and A. Kawamoto, J. Phys. Soc. Jpn. **84**, 084711 (2015).
[22] T. Yamamoto, M. Uruichi, K. Yamamoto, K. Yakushi, A. Kawamoto, and H. Taniguchi, J. Phys. Chem. B **109**, 15226 (2005).
[23] M. Maksimuk, K. Yakushi, H. Taniguchi, K. Kanoda, and A. Kawamoto, J. Phys. Soc. Jpn. **70**, 3728 (2001).
[24] M. Hemmida, H.-A. Krug von Nidda, B. Miksch, L. L. Samoilenko, A. Pustogow, S. Widmann, A. Henderson, T. Siegrist, J. A. Schlueter, A. Loidl, and M. Dressel, Phys. Rev. B **98**, 241202(R) (2018).